Twentieth Symposium (International) on Combustion/The Combustion Institute, 1984/pp. 1619–1628

COMBUSTION OF WOODEN SPHERES—EXPERIMENTS AND MODEL ANALYSIS

H. S. MUKUNDA, P. J. PAUL, U. SRINIVASA, AND N. K. S. RAJAN
Department of Aerospace Engineering
Indian Institute of Science
Bangalore-560 012, India

Studies on combustion of wooden spheres have been made towards understanding their role in wood gas generators. Experiments on 0.01, 0.015, 0.02 and 0.025 m dia spheres show two regimes of combustion—flaming and glowing. During flaming combustion, the sphere decreases in diameter by about 10% and loses 75–80% of its weight, this reduction being related to loss of volatiles only. Simulation experiments performed by inert heating of the wooden spheres to temperatures of about 350° C to cause loss of volatiles confirms the above result. The glowing zone combustion involves the remaining weight loss of 20% and diameter variation following the d^2-law. The mass loss correlations follow mass loss rate (kg/s) = $k \cdot$ diameter (m), $k = 7 \times 10^{-4}$ for flaming zone and 7×10^{-5} for glowing zone. A theory for flaming combustion involving the movement of an exothermic pyrolisis front into the sphere and other elements similar to droplet combustion theory has been evolved. The theory of glowing combustion of the porous char has been evolved following the model description of Howard. Both the theories include augmentation of heat and mass transfer due to free convection in an approximate way. Predictions from both the theories show that combustion times and weight loss time plots are represented reasonably well by the theories.

Introduction

Combustion of liquid fuel spheres has been investigated extensively due to many possibilities of technological applications. Spherical geometry particularly under zero-g conditions offer an excellent model for analytical treatment and has been treated by several researchers (See Krier and Foo [1] for a review). Studies of polymeric fuel spheres have also been conducted in recent times [2, 3, 4]. However the behavior of cellulosic materials and of natural polymers like wood in the form of spheres has not been examined adequately. As a matter of fact the authors know only of the work of Kuwata et al [5] which is on paper spheres.

Combustion of wood in the form of cylinders has been studied by Murthy and Blackshear [6, 7]. They mainly concentrate on elucidating the internal details of combusting wood, like the pyrolisis and char zones. Though their studies and those of Roberts [8, 9] have brought out many features regarding the combustion of wood, there does not appear to be a comprehensive theory of the combustion of wood. Some observations of Roberts [8b] on the analysis of combustion of wood are discussed later.

The objectives for the present work, therefore, are to obtain basic experimental data on spheres of wood and to construct an analysis to explain the results of the experiments by taking into account the principal features of combustion.

The Experiments

The combustion of wooden spheres of 0.01, 0.015, 0.02 and 0.025 m dia was performed at laboratory ambient conditions (1 g). A large number of spheres were turned out of an available stock of teak wood physically verified to be free of knots and other defects. The spheres were dried in an oven at 120° C for about 24 hours and their weights noted after cooling them in a dessicator. They were dried again in the oven for 8 hours, cooled and weighed. If, for a given sample, there was no difference between the two weights, it was taken that the sample was dry. Measurement of the weights of the sample before and after the introduction into the oven showed that they had about 10% moisture and the drying process ensured that this moisture was driven away.

The samples were later characterized for their density and combustion experiments conducted. The samples mounted on a fine needle with the needle in horizontal position were ignited using a flame from a spirit lamp. The time required to ignite the 0.025 m dia sample did not exceed 10 s and for lower

diameter samples proportionately less. The combustion process was clocked from the moment the flame enveloped the samples. The ignition time was less than 10% of the time the enveloped flame remained on the spheres and less than 2% of the time for complete consumption of the sphere. The combustion process would be quenched by dipping the combusting sphere into water. The quenched samples would be dried completely by a process similar to the one mentioned earlier, dimensions measured and weighted afterwards. More than 20 samples of the same diameter were burnt for different durations to obtain sufficient number of data points. During the flaming period, measurements of flame temperature and flame radius were carried out as well.

The combustion process was observed to be consisting of two phases. First phase in which a gaseous flame envelope the sphere in a steady manner resembles the classical droplet combustion. The source of fuel for the flame comes from the gases due to pyrolysis of wood. The second phase has no gaseous flame and the charred wood decreases in diameter with a corresponding coating of ash on the outer surface. This region is dominated by the combustion of porous charcoal with oxygen diffusing from the environment. While the completion of the flaming zone combustion appeared to lead to charcoal entirely in most of the cases, the large diameter samples (0.025 m) had problems of nonuniform completion of flaming combustion in a few cases and charring was not complete even after flaming had stopped. Several of the observations made during the tests are qualitatively similar to those made by Kuwata et al. [5] in the case of cellulosic spheres.

It is important to bring out that during the experiments, there was no fracture of the specimens and the specimens lived through the entire burn time without any observable cracks in all the experiments conducted here. The point made by Roberts [8, 9] that cracks are significant in modelling combustion of wood may be relevent in large sizes only.

The Experimental Results

All the results of $(d/d_o)^2$ and (w/w_o) are plotted with non-dimensional time (τ) in Fig. 1. The time coordinate τ is defined by $\tau = \tilde{t}(k/\rho c_p)_g/(d_o^2/2)$. The quantity $\tilde{t}$ is the time corrected for sample diameter and weight variations at a fixed nominal diameter. It is defined by $\tilde{t} = t/[(d_o/\bar{d}_o)^2\rho_o/\bar{\rho}_o]$ where quantities with bar refer to mean values and subscript o refer to initial values. The coordinate is essentially based on burn time varying like d_o^2, the classical d^2 law. The results show some scatter with a tendency for the data points of larger diameters to be below those of small diameters. This is thought

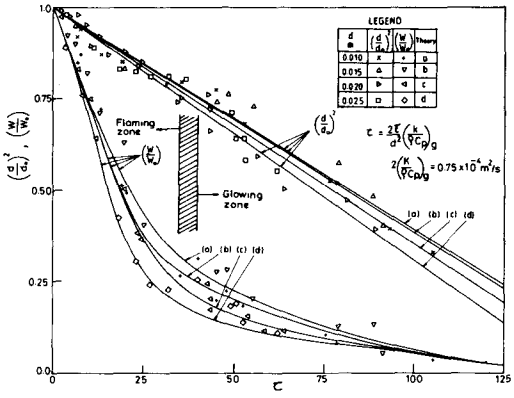

FIG. 1. Variation of diameter squared and weight ratios with nondimensional time. Lines show theoretical predictions. Each data point corresponds to one test for the specified duration.

to be due to free convection ignored in the choice of time coordinate. Others like Kuwata et al[5] assume a variation like $t_b \sim d^{1.85}$ whose inclusion in the coordinate, τ would have probably reduced the variation.

The flaming and glowing zones are delineated on the figure. Typical flaming times for all samples lie between $\tau = 35$–45. The d^2 and weight reduction at this stage are about 20–25% and 75–80% respectively. The variation of d^2 seems linear with time throughout the two zones of combustion. Kuwata et al [5] observed d^2 laws with different constants in the two zones for cellulose. The single constant observed here for wood may be due to difference in composition and no other fundamental feature can be ascribed to it. In order to verify this hypothesis, samples were kept in an inert environment at temperatures of 400° C for several hours, and dimensions and weight loss were measured. The diameter decreased by 9–12% and the weight loss by 75–77% in all the twelve experiments conducted for this purpose on the various diameter samples. It therefore appears that the processes of dimensional change (and of course, weight loss) are due to loss of volatiles, with flame being the primary source of heat.

The weight remaining after flaming (about 20–25%) is lost in the glowing zone due to porous charcoal oxidation by ambient oxygen. The density of the porous char (not shown in the Fig.) also decreases by 10–15% during the glowing period. This indicates the possibility of internal reactions with the oxygen diffused from the outer surface through the porous structure. Simple curve fits show that $\dot{m}$ (in kg/s) is about $7 \times 10^{-4}\ d$ in the flaming zone and $7 \times 10^{-5}\ d$ (d in m) in the glowing zone.

Measurements of flame to sphere diameter ratio show them to be in the range of 1.5–1.8 and are

consistent with similar results on liquid droplets (~0.012 m dia) obtained by Agoston et al [10]. Measured flame temperatures are about 1400° C and the core and surface temperatures increase with time as shown in Fig. 2 for one case. The core temperature (T_o) was measured by introducing a 100 μm dia Chromel-Alumel thermocouple into the center of the sphere through a 200 μm dia hole. The measured temperatures were corrected for conduction gain by conducting subsidiary experiments. Surface temperature (T_s) was measured by the same thermocouple by keeping it pressed against the bottom surface during the combustion. T_o and T_s seem to build up to 650 K and 960 K, respectively.

The Model

Based on the experimental observations noted above, a model for the analysis of combustion processes is developed. Figure 3 summarizes the essential elements of the model. There are four regions in the flaming zone. The region I constitutes the virgin material, region II the charred wood, region III the gas phase between the flame and the char surface occupied by the fuel gases and combustion products and region IV the ambient atmosphere outside the flame. The regions I and II are separated by the pyrolysis front which is assumed to be thin because the pyrolysis rate has high activation energy (~30 kcal/mole) and hence the pyrolysis occurs over a small range of temperature.

One of the important aspects concerning pyrolysis front is whether it is endothermic or exothermic. While Murthy and Blackshear [6] seem undecided about the nature of decomposition, Murthy [12] concludes from his analysis that the pyrolysis must be endothermic. Roberts [9] in a slightly earlier work has devoted an entire paper to this subject and shows from a careful examination of earlier data that at ambient pressures, particularly in situations relevent to combustion, the decomposition is exothermic and at sub-atmospheric pressures it could be endothermic. The exothermicity has been deduced to be about 160–240 kJ/kg. The present paper assumes pyrolisis to be exothermic based on the earlier mentioned evidence. Because of this reason the classical results of liquid fuel droplet combustion cannot be directly used in the case of wood combustion and there is need for the construction of a separate analysis. In the following, the analysis of flaming and glowing zones are described separately.

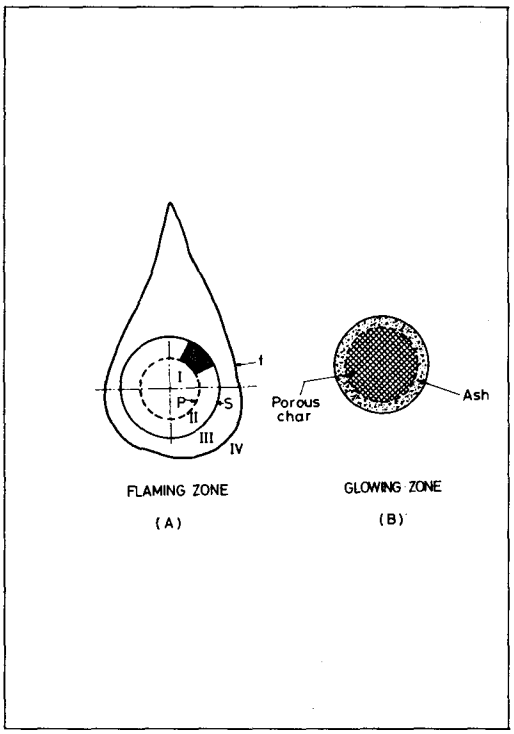

FIG. 3. The model—elements.
Region i : Virgin wood (p = pyrolysis front)
Region ii : Charred region (s = surface of wooden sphere)
Region iii : Gaseous zone of fuel vapours and product (f = flame zone)
Region iv : Ambient atmosphere

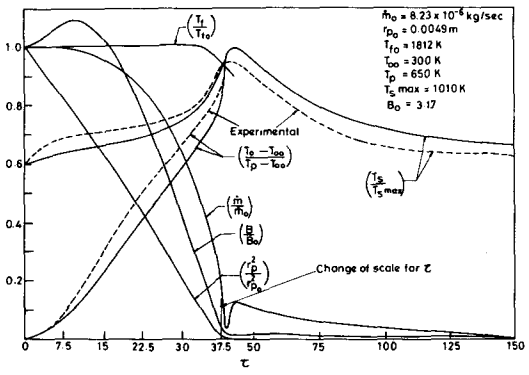

FIG. 2. Variation of combustion parameters with time. (Experiment and Theory).

Flaming Zone Analysis

The flaming zone consists of four regions described earlier. Region I is dominated by transient conduction. The governing equation for $T(r,t)$, $0 \leq r \leq r_p(t)$ is

$$T_t = \alpha_\omega (r^2 T_r)_r / r^2 \qquad (1)$$

where subscripts t and r refer to partial derivatives with respect to t and r. The initial and boundary conditions are $T(r,0) = T_{oo}$ and

$$(T_r)_{r=o} = 0 \quad \text{and} \quad T(r_p,t) = T_p \qquad (2a,b,c)$$

where T_p is the specified pyrosisis temperature. The phenomena of heat and mass transfer in the regions II, III and IV can be taken to be quasisteady based on the fact that the rate of movement of the pyrolysis front is very small compared to the gas velocities (~1/100 at the most). The governing equations are

$$\frac{\dot{m}c_p}{4\pi r^2} T_r = \frac{1}{r^2}(kr^2 T_r)_r \qquad (3)$$

and

$$\frac{\dot{m}}{4\pi r^2}(Y_i)_r = \frac{1}{r^2}(D\,\rho\, r^2 Y_i)_r \qquad (4)$$

The species considered are fuel ($i = f$), oxidiser (O), product (P) and inert (in). In writing the above equations gas phase kinetics has been neglected because thin flame approximation has been invoked. The thermodynamic and transport properties are being treated constant throughout the flow field. Relaxing this assumption increases complexity of algebra, and is not being attempted here. It will be assumed in the treatment to follow that Lewis number is unity. The essential features of the model namely transient conduction in virgin wood and quasisteady convective dominated flow in char and gas phase seem consistent with the observations of Roberts [8].

The interface and boundary conditions are

$$k\,T_r]_{r_p^-}^{r_p^+} = H_d\, m/4\pi r_p^2, \qquad (5a)$$

$$D\,\rho\,Y_{fr}]_{r_p^-}^{r_p^+} = (Y_{fp} - Y_{fp}^-)\,\dot{m}/4\pi r_p^2 \qquad (5b)$$

$$k\,T_r]_{r_s^-}^{r_s^+} = \dot{R}'', \quad D\,\rho\,Y_{fr}]_{r_s^-}^{r_s^+} = 0 \qquad (6a,b)$$

$$k\,T_r]_{r_f^-}^{r_f^+} = H_v\,D\,\rho\,Y_{fr}]_{r_f^-}^{r_f^+}, \qquad (7a)$$

$$D\,\rho\,Y_{fr}]_{r_f^-}^{r_f^+} = D\,\rho\,Y_{or}]_{r_f^-}^{r_f^+}/s \qquad (7b)$$

and

$$Y_o(\infty,t) = Y_{oo} \quad \text{and} \quad T(\infty,t) = T_{oo} \qquad (8a,b)$$

The relations noted above in Eqns. (5–7) are the flux conditions at the pyrolisis front, surface of the sphere and the flame. Y_{fp}^- in Eqn. (5b) refers to the fraction of volatiles in the virgin material. It is taken as 0.8 from the data available [12]. $\dot{R}''$ refers to the radiant exchange at the surface of the sphere due to radiant flux input from the flame and the loss of heat due to radiation from the surface. Both can be non-insignificant because the relative emissivities of the surface and the gaseous flame zone are widely different (1 for the surface and ~0.01–0.02 for gaseous flame front). It is written like

$$\dot{R}'' = -\epsilon_s\sigma(T_s^4 + \epsilon_f\, T_f^4) \qquad (9)$$

where ϵ_s and ϵ_f refer to emissivities at the surface and flame front respectively. Condition (7a) refers to the flame heat release relationship and (7b) refers to the flux ratio of fuel and oxidizer being in stoichiometric proportions, the classical flame surface location relationship.

Solutions

The solution for the transient conduction problem is obtained as shown in Appendix I. It can be written as

$$(T - T_{oo}) = \frac{(T_p - T_{oo})}{z}\frac{I(z;\, s_1,\, s_2)}{I(1;\, s_1,\, s_2)} \qquad (10)$$

where

$$z = r/r_p(t), \quad s_1 = r_p^2/4\alpha_\omega t, \quad s_2 = \dot{m}c_p/8\pi r_p k_\omega, \qquad (11a,b,c)$$

and

$$I = \int_0^z \exp[-(s_1 - s_2)(1 - x)^2 - 2s_2(1 - x)]dx \qquad (12)$$

The flux $k_\omega T_r]_{r_p^-}$ can be obtained as

$$kT_r]_{r_p^-} = \frac{k(T_p - T_{oo})}{r_p}\left[\frac{1}{I(1;\, s_1,\, s_2)} - 1\right] = \frac{k(T_p - T_{oo})}{r_p} f(s_1,\, s_2) \qquad (13)$$

The integral I has been obtained numerically for a wide range of parameters, $0 \le s_1 \le 10$ and $0 \le s_2 \le 2$ and the results have been curve fitted in terms of $f(s_1,s_2)$ as

$$f(s_1,s_2) = (0.663s_2 + 0.266s_2^2) + (0.356 + 0.0831s_2 + 0.016s_2^2)s_1 - (0.0049 + 0.0537s_2)s_1^2 \qquad (14)$$

The core temperature T_o can be obtained by taking the limit of the solution (10) as $z \to 0$. This gives

$$(T_o - T_{oo}) = (T_p - T_{oo}) \cdot \frac{\exp\{-(s_1 + s_2)\}}{I(1; s_1, s_2)} \quad (15)$$

In regions II, III and IV, the independent coordinate is subjected to the classical exponential transformations like

$$\eta_1 = \exp\left[\frac{\dot{m}c_p}{4\pi k}\left(\frac{1}{r_p} - \frac{1}{r}\right)\right], \quad r_p \le r \le r_s \quad (16a)$$

$$\eta_2 = \exp\left[\frac{\dot{m}c_p}{4\pi k}\left(\frac{1}{r_s} - \frac{1}{r}\right)\right], \quad r_s \le r \le r_f \quad (16b)$$

$$\eta_3 = \exp\left[\frac{\dot{m}c_p}{4\pi k}\left(\frac{1}{r_f} - \frac{1}{r}\right)\right], \quad r_f \le r \le \infty \quad (16c)$$

The governing equations under the above transformations will lead to equations with the second order derivative being zero. The linear solutions in η can be written down as

$$(T - T_p)/(T_s - T_p) = (Y_f - Y_{fp})/(Y_{fs} - Y_{fp}) = (\eta_1 - 1)/(\eta_{1s} - 1) \quad (17)$$

$$(T - T_s)/(T_f - T_s) = (Y_{fs} - Y_f)/Y_{fs} = (\eta_2 - 1)/(\eta_{2f} - 1) \quad (18)$$

$$(T_f - T)/(T_f - T_o) = Y_o/Y_{oo} = (\eta_{3\infty} - 1) \quad (19)$$

where Y_{fp} and Y_{fs} refer to the fuel mass fraction at the pyrolysis front (r_p^+) and surface of the sphere (rs), $\eta_{3\infty}$ refers to η_s as $r \to \infty$.

In obtaining the solutions, $kT_r]_{r_s^+}$ needs to be evaluated carefully because in the present situation free convective heat transfer cannot be ignored. The large sizes of the wooden sphere implies that the Grashof number is typically of the order of 1000–20,000. The effect is included by following the treatment of Agoston et al [10]. The enhancement in heat transfer is presented as

$$\frac{N_u}{N_{uo}} = 1 + 0.17\,Gr^{0.3}\,B^{-0.44} \quad (20)$$

where Grashof number,

$$Gr = g\,d^3(T_m - T_b)/T_b\nu_d^2, \quad (21)$$

T_m and T_b refer to mean temperatures defined in Reference 10, ν_d refers to the kinematic viscosity evaluated at a mean temperature. B is the transfer number defined by

$$B = \dot{m}c_p/4\pi r_s^2 h_m \quad (22)$$

with h_m refering to the heat transfer coefficient. The above definition of B matches with the definition in terms of enthalpies when there is an endothermic phase change.

N_{uo} can be expressed in terms of B as [10]

$$N_{uo} = \frac{2\ln(1 + B)}{B} \quad (23)$$

Using the definition $Nu = h_m\,d/k$ and the definition of heat flux, $\dot{q}'' = kT_r]_{r_s^+}$ as

$$\dot{q}'' = h_m\left(c_pT_\infty + \frac{H_vY_{oo}}{s} - c_pT_s\right) \quad (24)$$

the heat transfer condition can be written as

$$k\,T_r|_{r_s^+} = \frac{\dot{m}c_p}{4\pi r_s^2}\cdot\frac{1}{B}\left[T_\infty - T_s + \frac{H_cY_{oo}}{s\,c_p}\right] \quad (25)$$

where H_c is the heat of combustion/unit mass of the volatiles. Equations (23) and (22) can be used to obtain

$$\frac{\dot{m}c_p}{4\pi k r_s} = \ln\eta_s = \ln(1 + B)\,(1 + 0.17\,Gr^{0.3}\,B^{-0.44}) \quad (26)$$

Eqn (26) retains a structure in which, if $Gr \to 0$, the classical results of droplet combustion are recovered. The boundary conditions can be transformed and solutions utilized to obtain the relationships for various unknowns. These relations are

$$\eta_p = \exp\left[\frac{\dot{m}c_p}{4\pi k r_p}\right], \quad \eta_s = \exp\left[\frac{\dot{m}c_p}{4\pi k r_s}\right] \quad (27a,b)$$

$$\eta_{1s} = \eta_p/\eta_s,$$

$$\eta_{2f} = \eta_s/\eta_{3\infty}, \quad \eta_{3\infty} = 1 + C \quad (28a,b,c)$$

$$T_s = \frac{T_p}{1 + B(1 - \eta_s/\eta_p)} + \frac{T_o + H_vY_{oo}/sc_p}{1 + B/(1 - \eta_s/\eta_p)} - \frac{\dot{R}_1''B}{1 + B/(1 - \eta_s/\eta_p)} \quad (29)$$

$$T_f(1 + C)(\eta_s - 1) = \eta_sCT_s + (\eta_s - 1 - C)(T_o + H_vY_{oo}/sc_p) \quad (30)$$

$$\dot{R}_1'' = \sigma\epsilon_s(T_s^4 - \epsilon_f T_f^4)4\pi r_s^2/\dot{m}c_p \quad (31)$$

$$\frac{4\pi r_p k_\omega}{\dot{m}c_p} f(s_1, s_2) = \frac{H_d}{c_p(T_p - T_{oo})} + \frac{(T_s - T_p)}{(T_p - T_{oo})(\eta_{1s} - 1)} \quad (32)$$

$$\frac{dr_p}{dt} = -\frac{\dot{m}}{4\pi r_p^2\rho_p} \quad (33)$$

In order to obtain the solutions from equations 26–33, the parameters namely r_s and char density need to be specified apart from other thermodynamic and transport properties. From the experimental observations mentioned earlier, it is clear that r_s in the flaming zone decreases because of dimensional changes due to loss of volatiles. This is accounted for by assuming a d^2-law in terms of r_p^2 like $r_s^2 = [1 - r_p^2/r_p^2(t = 0)]r_s^2(t = 0)$. Char density is known from measurements as 170 kg/m^3. This is set into the calculation procedure to obtain mean density of the wood at any time.

The calculation procedure involves iteration and starts with specification of r_s and $r_p = 0.99\ r_s$ to start with. Further, the time t, is set at a value between 5–10 s to take account of initial temperature profiles inside the solid built up by ignition source. The values of η_p, η_s, η_{1s}, $\eta_{3\infty}$, η_{2f}, B, T_s and T_f are computed for an assumed value of $\dot{m}$, with the determination of B and T_s requiring iteration. Equation (32) is finally used to complete the iteration cycle on $\dot{m}$. Once $\dot{m}$ is determined r_p at the next time step is obtained from (33) and the procedure is continued till r_p goes to zero.

Input Parameters

The values of various physical constants used are as follows

c_p = 1.4 kJ/kg °C, k = 0.063 W/m °C, k_ω = 0.168 W/m °C, ρ_p = 650 kg/m^3, ρ_{char} = 170 kg/m^3, T_p = 600–700 K, T_{oo} = 300° K, H_d = 160–200 kJ/kg, H_c = 16.0 MJ/kg, Y_{oo} = 0.232, s = 1.53, $\bar{Y}_{fp}$ = 0.8, ϵ_s = 1.0, ϵ_f = 0.02

Most of the parameters have been chosen from the available sources [7–9]. The pyrolysis temperature of 600–700 K has been chosen based on the TGA data available [13] which indicate that major loss in weight occurs around this temperature range.

The results of the computation are discussed along with those of glowing combustion subsequently.

Glowing Zone

The Condensed Phase

The processes occuring during glowing zone are one of porous char combustion involving diffusion of oxidiser into the pores, adsorption of the oxidiser at active sites, reaction with char, desorption of the product, CO_2 into the interior gas phase and diffusion of the product out of the sphere [14]. The analysis is restricted to one dimension since the properties like diffusivity and conductivity are effectively governed by gas properties and hence one-dimensional approximation is expected to be reasonable. The phenomena can be adequately described by the unsteady species and energy conservation relations

$$(\rho e_p Y_i)_t = (-\rho v\, r^2 Y_i + r^2 \rho \bar{D} Y_{ir})_r / r^2 + \dot{\omega}_i''' \quad (34)$$

$$(\rho e_p)_t = -\dot{\omega}_c''' \quad (35)$$

$$(\rho c_p T)_t = (-\rho v\, r^2 c_p T + r^2 \bar{k}\, T_r)_r / r^2 - H_e \dot{\omega}_c''' \quad (36)$$

where $\bar{\rho} = \rho_c(1 - e_p) + \rho e_p$. In the above equations, e_p is the porosity, $\dot{\omega}_i'''$ refers to volumetric reaction rate of oxidiser, product and inert. $\dot{\omega}_c'''$ refers to volumetric reaction rate of carbon. In the Eq. (34), the species considered are CO, CO_2, O_2 and N_2. The proportion between CO and CO_2 is obtained from considerations enunciated by Welsh and Chung [15] who have obtained an expression for the ratio in terms of equilibrium constant of $CO—O_2—CO_2$ reaction. The volumetric reaction rate is related to the heterogeneous reaction rate per unit surface area through the relationship

$$\dot{\omega}_c''' = \dot{\omega}_c'' S_g \rho_{ap} \quad (37)$$

where $S_g \rho_{ap}$ is the surface area per unit volume of the char. The ρ_{ap} in the above equations is the apparent density. The surface reaction rate for carbon is given by [14]

$$\dot{\omega}_c'' = -M_c S_1 S_2 X_{os} / (S_1 X_{os} + S_2) \quad (38)$$

where X_{os} is the mole fraction of oxygen at the surface, S_1 and S_2 are the rate constants defined by

$$S_1 = A_c P \exp (-E_1/RT)/\sqrt{2\pi M_{O_2} RT} \quad \text{(adsorption)} \quad (39)$$

$$S_2 = A \exp (-E_2/RT) \quad \text{(desorption)} \quad (40)$$

The diffusion coefficients and the thermal conductivity have been defined for the porous medium by [14, 6]

$$\bar{D} = \frac{e_p}{\tau}\left[\frac{1}{D} + \sqrt{\frac{9\pi M_g}{8 r_{pb} RT}}\right]^{-1} \quad (41)$$

$$\bar{k} = k_c(1 - e_p) + k \quad (42)$$

In the expression for D, τ refers to Torsuasity factor taken 1.5 following Ref. 15, the first term inside the parenthesis refers to inverse of gas phase diffusivity taken for oxygen in CO_2, the second term is the inverse of Knudsen Diffusion Coefficient dependent on pore radius r_{pb}. In the present calculations the Knudsen diffusion coefficient is about 50 times that of gas phase diffusion coefficient so that the effective diffusion coefficient is that in the gas phase only. The thermal conductivity is the average

of the solid and gas conductivities weighted volumetrically by porosity [6]. The variation of pore radius, r_{pb} with time is obtained by treating the pores as long tubes from the relation

$$\rho_c(r_{pb})_t = -\dot{\omega}_c'' \tag{43}$$

The pore radius and the surface area per unit volume ($S_g\rho_{ap}$) are related by

$$S_g\rho_{ap} = 2e_p/r_p \tag{44}$$

In order to obtain the mass flow rate of gases issuing out of the porous char consistent with the unsteady formalism, the equation of state $\rho = pM_g/RT$ is manipulated to obtain

$$(\rho e_p)_t\rho e_p/\bar{\rho} + (e_p)_t(1 - \rho_c e_p/\bar{\rho})\rho - M_g\Sigma(\rho e_p Y_i)_t/M_i - (\bar{\rho}c_pT)_t\rho e_p/(c_pT\bar{\rho}) = 0 \tag{45}$$

All the derivatives with respect to time in Eqn. (45) are replaced using Eqn. (34–36).

Gas Phase

The gas phase is treated quasisteady and reactions are neglected. The gas phase equations are the same as Eqn. (3) and (4) and the solution can be written as

$$\frac{T - T_{oo}}{T_s - T_{oo}} = \frac{Y_i - Y_{io}}{Y_{is} - Y_{io}} = \frac{1 - \eta}{1 - \eta_s} \tag{46}$$

where

$$\eta = \exp[-\dot{m}c_p/4\pi kr] \tag{47}$$

In obtaining the above solution Lewis number has been taken as unity. The fluxes of mass and heat obtained from above need to be modified to include free convection. The empirical formulation to include free convection uses relations different from the earlier one (Eqn. 20) because the physical situation here is one of heated sphere only. Following Bird et al [16] the heat transfer and mass transfer coefficients including the effect of mass injection can be written as

$$Nu = \frac{B_o}{1 + \exp B_o}[2 + 0.6\,Gr^{1/4}Pr^{1/3}] \tag{48}$$

where

$$Gr = gd^3(T_s - T_\infty)/[(T_s + T_\infty)/2]\nu_m^2 \tag{49}$$

and

$$B_o = \dot{m}c_p/4\pi r_s^2 h_{mo} \tag{50}$$

$$h_{mo} = (2 + 0.6\,Gr^{1/4}Pr^{1/3})d/k \tag{51}$$

The flux of oxidiser and heat as influenced by free convection are evaluated from equations 48–51 as

$$D\rho(Y_o)_r]_{r=r_s^+} = Q(Y_{o\infty} - Y_{os}) \tag{52}$$

and

$$kT_r]_{r=r_s^+} = c_pQ(T_\infty - T_s) \tag{53}$$

where $Q = \dot{m}/4\pi r_s^2 \exp(-B_o)/[1 + \exp(-B_o)]$. In the absence of free convection the results from (52) and (53) will be same as obtained from Eqn. 46.

Initial, Interface and Boundary Conditions

The initial conditions at $t = 0$ are those obtained from the earlier analysis. The input data for the present calculations will be the temperature profile in the porous char. Since gas phase is treated quasisteady solutions stated earlier are valid.

The interface conditions at $r = r_s$ are one of continuity of fluxes of heat and mass. These are

$$kT_r]_{r_s^-}^{r_s^+} = D\rho Y_{ir}]_{r_s^-}^{r_s^+} = 0 \tag{54}$$

In Eqn. (54), the expression for $kT_r]_{r_s^+}$ and $D\rho Y_{or}|_{r_s^+}$ are obtained from Eqns. (52) and (53).

The Boundary conditions are,

$$r = 0, \quad T_r = Y_{ir} = 0$$
$$r \to \infty, \quad T \to T_{oo}$$
$$Y_o \to Y_{oo}, \quad Y_p \to 0, \quad Y_{in} \to Y_{ino} \tag{55}$$

Method of Solution

The solution calls for integration of the parabolic system of partial differential equations (34–36) subject to the initial and boundary conditions (54 and 55) along with the subsidiary relations (37–44). An interesting transformation of the independent coordinate which renders the difference equations into a conservative form and eliminates the singularities at $r = 0$ has been made. This calls for using volume elements instead of elements in r,

The equations become

$$(\rho e_p Y_i)_t = (-\dot{m}Y_i + D\rho(4\pi)^{2/3}(3v)^{4/3}Y_{iv})_v + \dot{\omega}_i''' \tag{56}$$

$$(\bar{\rho}c_pT)_t = (-\dot{m}c_pT + k(4\pi)^{2/3}(3v)^{4/3}T_v)_v - H_c\omega_i''' \tag{57}$$

where $v = 4\pi r^3/3$.

Two methods of integrating the partial differential equations namely, method of lines, with Gear Hindmarsh package as well as Runge Kutta Gill routine and Crank Nicholson scheme were attempted and the latter was adopted as it turned out to be computationally far superior to the other methods. The volume range has a step size of 0.05–0.01 and the time step chosen varies from 0.5–1 s. Typical computation times for a burn time of 1 s is about 30 s of CPU on DEC1090 computer.

Input Parameters

While the parameters of gas phase are about the same as noted earlier, the other parameters are as below:

A_c = 1/150, E_1/R = 1700 K, E_2/R = 20,000 K A_f = 0.0875 moles/m^{2}s, $r_{pb}(t = 0)$ = 50 μm, k = 0.042 W/m°C, H_c = 32.600 MJ/kg, ρ = 1900 kg/m^3, Pr = Sc = 0.74

These parameters are about same as given by Howard [14].

Results and Discussion

Results of computations of both flaming and glowing zones are presented in Fig. 1 as lines. The figures show that weight loss and diameter reduction increase with initial diameter, an effect caused by free convection. The predictions generally cover the band of experimental results and the comparison appears good. The comparison of d^2 variation in the flaming zone is only a partial test because the $(d/d_o)^2$ vs $(r_p/r_{p_o})^2$ relationship has been invoked. In the flaming zone, H_d, k/c_p and c_p are important parameters affecting the predicted weight loss profile. A 10% increase in each of these causes −5%, −3% and 20% change in the flaming time. The transient term (due to s_1) is significant (more than 10%) up to 70% of the flaming time and during the rest of the time, the convective term (s_2) dominates. Parameters like ϵ_f, Y_{fp}^- have marginal influence in the predictions of weight loss. Results of temperatures shown in Fig. 2 indicate that the predictions of both surface and core temperatures are lower by about 10% compared to the measured values in the flaming zone. In the glowing zone, the surface temperatures appear overestimated by about 10%. These differences are not very significant considering the accuracy of measurement and the approximation of the analysis involving the temperature distribution. Other results of detailed parameters are also seen in Fig. 2. The variation of $\dot{m}$ indicates that it is about same till about half the flaming period, but falls steeply towards the rest of the flaming period. In the early part of the glowing zone, the mass loss rate is about one tenth of that during the initial flaming period, and falls off slowly during the rest of the glowing period which occupies thrice the time taken for flaming. The transfer number B goes up by about 10% before falling off steeply during the latter half of the flaming period. Its magnitude is about 3 and it should be understood in the frame work of Eqn. 22 particularly because the phase change (due to pyrolisis) is exothermic. The variation of radius of pyrolisis front seems to obey rather nearly the d^2-law, excepting that the time of flaming (which appears in the equivalent law for r_p^2) is determined by the analysis involving exothermic pyrolysis and other unsteady features unlike in the classical droplet combustion where quasisteady approximation would be satisfactory.

The results of sensitivity analysis in the glowing zone indicated that gas phase diffusivity and reaction rate parameters of adsorption are important in influencing the mass loss rate. A 10% increase in diffusivity causes 8% variation in mass loss rate. Increased diffusivity causes greater availability of oxygen to the inside. A 10% increase in conductivity causes a reduction of about 2% in mass flow rate primarily by enhancing the heat losses as well as broadening the temperature profile inside the porous sphere. The reaction parameters of desorption process have negligible influence as this process is not rate controlling.

If computations are made for the diffusion limited case ignoring free convection, $\dot{m}$ is underestimated by 50% in comparison with observed results. Inclusion of free convection heat transfer enhances the burn rate to 130% of the observed rate. This implies that reaction kinetics must be playing an important role in modulating the burn rate of the char. Computations show that the reaction is concentrated around 80–85% of the local radius and the reaction zone accounts for 25% of the volume of the sphere. The peak reaction rate of carbon is about 10,000 kg/m^{3}s.

Summarizing, the present study presents a comprehensive picture of combustion of wooden spheres. The combustion experiments have brought out, weight loss and diameter variations and variation of temperatures at surface and the core with time of combustion during the flaming and glowing periods. The models for both the phenomena have been subjected to analysis and the results using parameters well established in literature lead to satisfactory prediction of most of the observed features in both the flaming and glowing zones.

Nomenclature

A, A_c	Reaction rate constants given by Eqns. (39) and (40)
B	Transfer number defined by Eqn. (22)
B_o	Transfer number defined by Eqn. (50)
C_p	Constant pressure specific heat (kJ/kg°C)

d	Sphere diameter (m)
D	Diffusion coefficient (m^2/s)
$\bar{D}$	Effective diffusivity of char
e_p	Porosity
E_1, E_2	Activation Energies of char reaction, Eqn. (39) and (40)
Gr	Grashof number defined by Eqn. (21) and (49)
h_m	Heat transfer coefficient ($W/m^{2o}C$)
H_d	Heat of decomposition of Wood (kJ/kg)
H_v	Heat of combustion of Volatiles
H_c	Heat of combustion of Carbon
k	Thermal conductivity of gas (W/m°C)
k_ω	Thermal conductivity of Wood
$\bar{k}$	Mean thermal conductivity in char zone
k_c	Thermal conductivity of char material
Le	Lewis number ($D \rho c_p/k$)
m	Mass flow rate of gases from the solid (kg/s)
N_u	Nusselt number ($=h_m d/k$)
$\dot{q}''$	Heat flux (W/m^2)
r	Radial coordinate (m)
r_f	Flame radius
r_p	Radius of pyrolisis front
r_{pb}	Pore radius in char
R	Universal gas constant (J/kg-mole°C)
$\dot{R}''$	Radiant flux (W/m^2)
s	Stoichiometric ratio of volatiles combusting with air
s_1, s_2	Constants defined in Eqns. (11b,c)
S_g	Surface Area of unit mass of char (m^2/kg)
T	Temperature (K)
Y_i	Mass fractions of species i
$\dot{\omega}_i'''$	Volumetric reaction rate (kg/m^3s)
$\dot{\omega}_i''$	Surface reaction rate (kg/m^2s)
Z	$r/r_p(t)$
ρ	Density (kg/m^3)
$\bar{\rho}$	Average density in porous zone
ρ_{ap}	Apparent density of porous char
η, η_1	Coordinate transformations defined in Eqns. (16a–16c)
η_2, η_3	
τ	Nondimensional time

Subscripts

f	Flame front
p	Pyrolisis front
r	Derivative with respect to r
s	Surface of the sphere
o	Free stream

Appendix

Approximate solution of transient conduction equation

Equation (1) is first transformed using $\Psi = (T - T_{oo})r$ into $\Psi_t = \alpha_\omega \Psi_{rr}$. The independent coordinates are transformed as $t = t$ and $\eta = (r_p - r)/2\ r_p\sqrt{\alpha_\omega t}$. This gives $\Psi_t - \eta\Psi_n/2t + (\eta - 1/2\sqrt{\alpha_\omega t})\ \Psi_n|r_p'|/r = \Psi_{\eta\eta}/4r_p^2 t$ where r_p' refers to derivative of r_p with respect to t defined in terms of $\dot{m}$ by Eqn. 33.

There are two transient effects in the above equation. One of these is due to boundary moving inwards and the other due to unsteady conduction. It is now assumed that all unsteadiness is absorbed in η and the derivative of the term Ψ_t is small compared to others. This assumption leads to similarity solution in plane one dimensional case. It will be approximate in the present spherically symmetric case. Time, t is treated as a parameter in the above equation. The resulting solution after reverse transformations from η to r, Ψ to T is the one stated in Eqn. 10.

Acknowledgment

The experimental work reported in this paper is supported by a project on "Wood gas generators for diesel engines with power less than 10 HP" administered by Karnataka State Council of Science and Technology.

REFERENCES

1. KRIER, H. AND FOO, C. L., Oxidation and Combustion Reviews *6*, p. 111 (1973).
2. ESSENHIGH, R. H. AND DRIER, W. L., Fuel, *48*, p. 330 (1969).
3. RAGHUNANDAN, B. N. AND MUKUNDA, H. S., Fuel, *56*, p. 271 (1977), Also see Combust and Flame, *30*, p. 71 (1977).
4. OKAJIMA, S., YAMAGUCHI, S. AND ABE, K., Ignition and Combustion of Polymeric Spheres in high temperature atmosphere., Bull. College of Engineering, Hosei Uni., Tokyo, *17*, p. 87 (1981).
5. KUWATA, M., STUMBAR, E. AND ESSENHIGH, R. H., Twelfth Symposium (International) on Combustion p. 663 (1969).
6. MURTHY KANURY, A. AND BLACKSHEAR, P. L., Combustion Science and Technology, *1*, p. 339 (1970); also see ibid, *2*, p. 5 (1970).
7. BLACKSHEAR, P. L. AND MURTHY KANURY, A., Combustion Science and Technology, *2*, p. 1 (1970).
8. ROBERTS, A. F., Combustion and Flame, *14*, p. 261 (1970).
9. ROBERTS, A. F., ibid, *17*, p. 79 (1971); also see Thirteenth Symposium (International) on Combustion, p. 893 (1971).
10. AGOSTON, G. A., WOOD, B. J. AND WISE, H., Jet Propulsion p. 181 (1958).
11. MURTHY KANURY, A., Combustion Science and Technology, *5*, p. 135 (1972).
12. TILLMAN, D. A., RUSII, A. J. AND KITTO, W. D.,

Wood Combustion, Principles, Processes and Economics (1981).
13. MILNE, T., Pyrolisis—The thermal behaviour of biomass below 600 C, Chapter 6.
14. HOWARD, J. B., Combustion of carbon with oxygen. MIT Report (1967).
15. WELSH, W. E. JR. AND CHUNG, P. M. Proc. Heat Transfer and Fluid Mechanics Institute, p. 146 (1963).
16. BIRD, R. B., STEWART, W. E. AND LIGHTFORT, E. N., Transport Phenomena, p. 413 and p. 663, John Wiley and Sons (1960).

COMMENTS

H. Takeda, University of Tokyo, Japan. The shape of the wood is initially spherical. But I suspect the shape becomes distorted from the sphere during combustion. Did you observe such distortion?

Would you tell me the definition of the diameter? Because I think the burning condition of the top of the sphere is different from the bottom.

Authors' Reply. The problem of distortion of the shape is present only in the case of liquids and polymers which liquify. No such problem is experienced in the case of wood spheres since the char which is structurally sound still remains. Consequently, the diameter measured along all lines through the centre will *remain the same.*

•

J. Quintiere, National Bureau of Standards, USA. In your analysis of the char glowing regime you accounted for porosity in the char. But you did not address the consequence of simultaneous reduction and conduction in the porous char. This implies a pseudo-conductivity. Could you comment on this omission?

Authors' Reply. The conductivity used in porous char analysis accounts for porosity as given by Eqn. 42.

•

S-J Ying, University of South Florida, USA. You claim that you have considered the free convection in the formulation, but you have used only one spatial coordinate (radius) in your equations. I do not see how a one dimensional model can be able to take care of the free convection. Please explain.

Authors' Reply. The model developed is essentially to estimate the mass loss rates of the spherical mass of wood. As long as the heat transfer rates coming to the surface are correctly modelled these estimates will be proper and the dependence on various physico-chemical parameters will be brought out properly.

Towards this end, the simplest thing is to treat a one dimensional model accounting for free convection through a correlation. This is what has been done in the paper.